Review

Review of Non-Classical Features of Deformation Twinning in hcp Metals and Their Description by Disconnection Mechanisms

Andriy Ostapovets [1,*] and Anna Serra [2]

[1] CEITEC-IPM, Institute of Physics of Materials, Czech Academy of Sciences, Žižkova 22, 61600 Brno, Czech Republic

[2] Department of Civil and Environmental Engineering, Universitat Politècnica de Catalunya, Jordi Girona, 1-3, C-2, Campus Nord, 08034 Barcelona, Spain; a.serra@upc.edu

* Correspondence: ostapov@ipm.cz; Tel.: +42-05-3229-0429

check for updates

Abstract: The study of deformation twinning has long history. However new, sometimes surprising, findings have shown that the phenomenon of deformation twinning still is not completely understood. During recent years, some debates are taking place in the scientific literature concerning deformation twinning mechanisms in metals with hcp structure. These debates deal with the importance of special twin boundary dislocations named disconnections, growth and nucleation of twins, non-Schmid behavior of twinning, difference of deformation produced by twins from simple shear. They invoked new propositions for atomistic mechanisms of deformation twinning. The purpose of this review is to compare the classical theories of interfacial defects with the new findings and prove that many of these findings can be understood in terms of these well-established theories. The main attention is paid to summarizing the explanations of different phenomena in terms of disconnection mechanisms in order to show that there is no contradiction between these mechanisms and the new findings.

1. Introduction

Mechanical (deformation) twinning is an important mechanism of plastic deformation in metals with hexagonal crystal structure [1–7], e.g., magnesium or titanium alloys. An increase of interest has been observed for twinning mechanisms in these materials during the last 10 years linked to the development of new lightweight materials for automotive and aerospace industry as well as materials for biomedical applications.

Since twinning is a common phenomenon in materials, its study has a long history [8]. It is worth to note that deformation twins are only a particular case of the objects, which are called "twins". For a general twin the so-called "crystallographic" definition can be provided, for instance as follows [9]: a twin involves two different configurations of a crystal, meeting at a plane, called the twin plane or composition plane, such that the positions of atoms in the two can be related by an isometry. In contrast, deformation twins can be defined in the following way [3]: a deformation twin is a region of a crystalline body, which has undergone a homogeneous shape deformation in such a way that the resulting product structure is identical with the parent but oriented differently. The twin is a reoriented part of material, which often has specific and well-defined orientation relative to the surroundings. The commonly observed symmetry relations between twin and matrix are reflection in twinning plane (K_1), rotation of π about twinning direction (η_1), reflection in the plane normal to η_1 or rotation of π about the normal to K_1 [2,7]. Other types of twins such as growth twins, annealing twins and transformation twins from phase transition can have different mechanisms of

formation in comparison to deformation twins. Deformation twinning plays a crucial role in plastic deformation of hcp materials. Consequently, the definition of deformation twinning as homogeneous shape deformation is important for the description of mechanical behavior of materials. On the other hand, the "crystallographic" description of deformation twins is also important to the recognition of the twin region by diffraction methods.

The characteristics of a deformation twin lead to the following constraints [3]: if the twin and matrix are to remain in contact, the deformation must be an invariant plane strain. Since the two structures are identical, there can be no volume change, so that the deformation must be a simple shear. Based on this, twins are identified by four crystallographic parameters (Figure 1). The invariant (undistorted) plane of this simple shear is denoted by K_1, and the direction of shear (lying in K_1) by η_1. K_1 is called the composition or twinning plane. The second undistorted (but rotated) plane of the simple shear is denoted by K_2 and the plane perpendicular to K_1 and K_2, by S. The plane S is called the plane of shear, and it contains η_1 and intersects K_2, in the direction η_2. A mode of deformation twinning is completely defined by the elements K_1 and η_2, but it is usual to quote the four elements K_1, η_1, K_2, η_2. Corresponding to this twinning mode there exists a conjugate (or reciprocal) twinning mode, with the same magnitude of shear, defined by the elements $K_{1'}$, $\eta_{1'}$, $K_{2'}$, $\eta_{2'}$ where $K_{1'} = K_2$, $K_{2'} = K_1$, $\eta_{1'} = \eta_2$, $\eta_{2'} = \eta_1$. K_2 and η_2 are thus called the reciprocal twinning plane and reciprocal twinning direction, respectively.
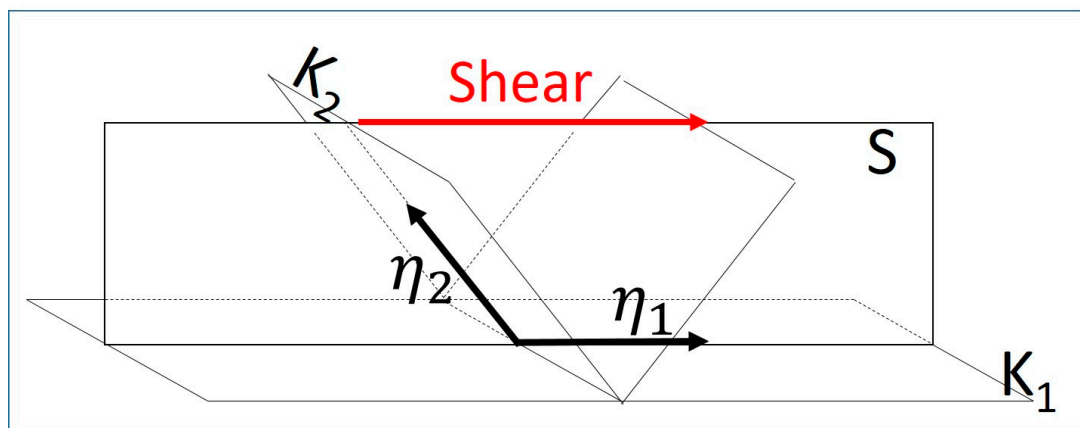

Figure 1. Illustration of twinning elements: K_1—twinning plane, η_1—twinning direction, K_2—conjugate twinning plane, η_2—conjugate twinning direction.

Recently, papers dealing with twinning mechanisms have brought a significant progress in the topic. New, sometimes surprising, findings have shown that the phenomenon of deformation twinning still is not completely understood. For instance, it was demonstrated that faceting of twin boundaries is quite common and real twinning interface does not necessarily coincide with K_1 plane [10–19]. The development of facets in twin boundaries were demonstrated in detail by atomistic simulations [10–12,15,17,18] as well as by experimental observations [13,14,16,19]. It was found that twin boundaries can be asymmetrical, e.g., basal-prismatic (BP) interface was widely discussed for $\{10\bar{1}2\}$ twin [10–12,14,18]. The main peculiarity of this twin, compared with the other twins in hcp metals, is that this twin is the most frequent, but the growth mechanisms at the atomic level of this twin are the same as for any other twin in the hcp metals. The fact that the macroscopic shape of the twin differs from the typical straight lamella is due to the existence of non-invariant facets, such as BP, as we describe below. This non-standard shape stimulated the development of new theories and many debates concerning atomistic mechanisms of deformation twinning are present in recent literature. These debates deal with the importance of special twin boundary dislocations named disconnections [20,21], growth and nucleation of twins [22–25], the possibility of non-Schmid behavior [26,27], deformation produced by twins e.g., inclinations from simple shear [28]. The purpose

of this review is to compare the classical theories of interfacial defects with the new findings and prove that many of these findings can be understood in terms of these well-established theories.

We begin with the comparison of bulk dislocations and twin boundary (TB) dislocations and the description of special TB dislocations, i.e., disconnections and their sources at the TB. Then we describe faceting as an aspect related to the invariance of the twin plane. The last section focuses on the $\{10\bar{1}2\}$ deformation twinning describing the concepts that, together with the plane invariance, have generated much debate such as zero shear and Non-Schmid behavior.

2. Dislocations and Disconnections

2.1. Crystal Dislocation Versus Twin Boundary Dislocation

Twin boundaries (TB), like grain boundaries in general, have intrinsic line defects with dislocation character. A TB dislocation that has, in addition, step character is named disconnection [20,21]. Like bulk dislocations, the characterization of the Burgers vector of a TB dislocation can be done by means of the Burgers circuit. It follows a comparison of Burgers circuits applied to a bulk dislocation and a TB dislocation.

Figure 2 presents a crystal dislocation (Figure 2a) and a TB dislocation, disconnection in this example, (Figure 2b) together with the corresponding Burgers circuits. In the case of a crystal dislocation, the reference configuration, where the circuit is reproduced, is the ideal crystal and the closure failure (Burgers vector) is equal to a translation vector of the crystal (Figure 2c). However, the situation is a bit different for a dislocation settled in the TB. The reference configuration is now a bicrystal that can be visualized by the dichromatic pattern [20], and the closure failure of the circuit is not a translation vector. The dichromatic pattern, shown in Figure 2d of $\{10\bar{1}2\}$ twin [29], is produced by superimposing twin and matrix lattice sites with a coincident. $\{10\bar{1}2\}$ plane; the lattice sites of each crystal were marked by white and black symbols respectively. Notice that the two atoms at each lattice site are not included.

Given the Burgers circuit, one can identify two translation vectors with common origin (the C point, for instance), so that the difference is the Burgers vector. This is valid for both cases. Although in the crystal dislocation both translation vectors (e.g., CS and CF) belong to the same lattice, and hence the difference is a crystal symmetry too, in the TB dislocation the translation vectors belong to different lattices, CS is in the white (upper crystal) and CF is in the black (lower crystal). In the latter case, the difference is not a translation vector and its magnitude can be much smaller than the Burgers vector of a crystal dislocation. In the case shown in Figure 2 the value of the Burgers vectors are a_0 and $0.152a_0$ for the crystal dislocation and disconnection respectively. Where a_0 is the hcp lattice parameter.

Thus, apart for the difference of Burgers vectors just described and the fact that grain boundary dislocations are confined to the grain boundary, bulk and grain boundary dislocations have the same characteristics, such as conservation of Burgers vectors, Frank rule for the energy balance of a dislocation reaction, etc.

2.2. Description of Disconnections

When two crystals are put together to produce a bicrystal, there are symmetries of each of them that are broken in the bicrystal. Then the line defects occurring at TB can be associated with these broken symmetries. A special defect exists in the TB described as a line defect that have both, dislocation, with Burgers vector b, and step character, with step height h. Such defect was called "disconnection" in order to distinguish it from TB dislocations without step. If the disconnection has appropriately oriented Burgers vector, it can glide along the TB; we name it twinning disconnection. A twinning disconnection glides under an applied stress due to its dislocation nature. This glide is accompanied by TB migration due to the boundary step associated with the disconnection. This chapter reviews the migration of twin boundaries due to glide of disconnections along the boundary. To do so, it is applied to the well-established theory of dislocations to the behavior of disconnections.

Figure 2. (**a**,**c**) Edge dislocation in an hcp single crystal with dislocation line along [1]. Crystal dislocation encircled by a Burgers circuit, which is reproduced in the perfect crystal below. Atoms are colored according to their energy. The circuit is plotted anticlockwise from S to F. The Burgers vector of the dislocation is indicated below the closure failure in red. It corresponds to a lattice vector $\boldsymbol{a}_0$. Projection in [1] direction. (**b**,**d**) disconnection in $\{10\bar{1}2\}$ twin boundary from atomistic simulations. The $\{10\bar{1}2\}$ twin boundary is indicated by red dashed line. The disconnection produces step in the boundary. The Burgers circuit is reproduced in the dichromatic pattern. It starts in the S point at the black crystal, and continues in white crystal from point C, which is common for both crystals. It continues to the point F. The vector FS is the Burgers vector of the disconnection. Projection in $\langle 1\bar{2}10 \rangle$ direction.

Let us illustrate the idea of disconnection with the case of the frequently discussed $\{10\bar{1}2\}$ twinning in magnesium. A two-layer step disconnection in $\{10\bar{1}2\}$ twin boundary is shown in Figure 3. As proved in the previous subsection by drawing a Burgers circuit, this step has dislocation nature. For a Burgers circuit on a high resolution transmission electron microscopy (HRTEM) image of the same disconnection, see reference [16]. Such proof is based on the definition of dislocation and leaves no room for debates such as "the corresponding Burgers vector is zero", as was claimed by some authors [28,30].

Figure 3. Disconnection in $\{10\bar{1}2\}$ twin boundary from atomistic simulations. The atoms are coloured according to their energy. Twin boundary lies along the plane containing red and dark blue atoms. The disconnection is settled in the step on the boundary. (Reproduced from [12], with permission from IOP publishing, 2014).

The motion of glissile disconnections produces two effects, on the one hand, it accommodates plastic deformation and, on the other hand, the motion of the step transforms one crystal at the expenses

of the other [31]. By this way, the TB is displaced and the twin may grow or shrink. Macroscopically, this is a mode of plastic deformation. At the atomic level, the motion of the disconnection produces displacements of the atoms at the core of the disconnection. These displacements include the shear associated to the dislocation character, s = $|b|/h$ (here b is Burgers vector, h—step height), and an additional rearrangement of atoms (shuffles) to restore the lattice transformed by the step [3,32,33]. Shuffles can be envisioned to be associated with the motion of the step part, and shear from the motion of the dislocation part. Figure 4 shows a dichromatic complex, where the two atoms of each lattice site are represented, with the total displacements of the atoms decomposed into shear (red) and shuffles (blue). Whereas the shear is cumulative, shuffles are local and affect only the atoms swept by the step [34]. This can be seen in Figure 4: the shear of layer 4 is four times the shear of layer 1, but the shuffles of layer 4 are the same as for layer 1. Notice that the net distortion of the crystal produced by shuffles is zero.
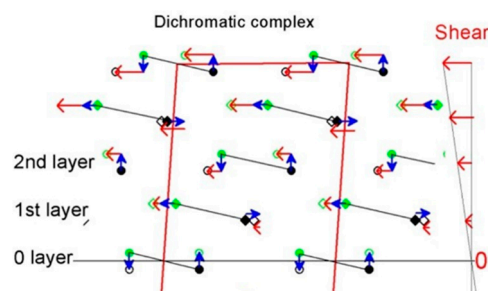
Figure 4. Dichromatic complex of the $\{10\bar{1}2\}$ twin with the displacements of atoms, produced by the passage of a disconnection, decomposed into shear (red) and shuffles (blue). (Reproduced from [32] with permission from Taylor & Francis Ltd., 2013).

2.3. Sources of Disconnections

Disconnections with small step height and small Burgers vector can reasonably be created as dipoles in pristine interfaces under a locally high stress concentration.

The interaction of the boundary with bulk dislocations can produce interfacial defects that act as sources of disconnections [29]. The residual defect produces disconnection dipoles in adjacent twin planes via stress concentrations. The mechanism is efficient for the twin growth if the source can move together with the boundary in a conservative motion, i.e., no atomic diffusion is needed [29] (see section "faceting of twin boundaries" for details). The mechanism happens in the main crystallographic structure (hcp, bcc and fcc) and depends on the crystallography of the interface and the energetic balance of the decomposition of Burgers vector. This twin thickening controlled by twin dislocation sources resulting from slip dissociations at twin interfaces is referred as slip-assisted [35]. Sources of disconnections in $\{10\bar{1}2\}$ twin boundary [29,36–38], in {112} twin boundary [39] and in {410} grain boundary [40] are examples for hcp, bcc and fcc crystals respectively. If the twin dislocation source does not require previous slip activity, the source is slip dislocation-independent [35]. Then the creation of disconnections occurs from sequential emission from grain boundaries, external surfaces or stress concentrators [41], cross-slip [42] and spontaneous formation of dipoles caused by fast propagation of twinning dislocations [43].

3. Faceting of Twin Boundaries

Some twin boundaries contain interface segments that are not invariant with respect to the twinning shear deformation. This situation can be easily understood if a 3-dimentional structure of twin is taken into account. The 3-dimentional object cannot have all its boundaries in coincidence with K_1 planes. One can expect that non-invariant interfaces can occur in twin tips or in the other irregularities in twin boundaries. In the last case, they can lead to faceting of twin boundaries, i.e., to the situation when twin boundary consists of segments with different crystallographic orientation.

The resulting interface either can coincide in average with K_1 plane or can be curved or irregular. A prominent example of such faceting is the occurrence of basal-prismatic facet in the $\{10\bar{1}2\}$ twin in hcp metals. This case is interesting also because the energy of $(0001)/\{10\bar{1}0\}$ interface is comparable to the energy of $\{10\bar{1}2\}$ boundary [12,18]. Due to this fact, abundant occurrence of the basal-prismatic interfaces was observed in hcp metals (e.g., magnesium and cobalt) both experimentally [44–49] and theoretically [10,11,18,48], which leads to significant inclination of twin interface from $\{10\bar{1}2\}$ plane. An example of faceted twin tip is shown in Figure 5 [44]. The similar faceted twin tip was also experimentally found in magnesium [14,48] or zinc [50].
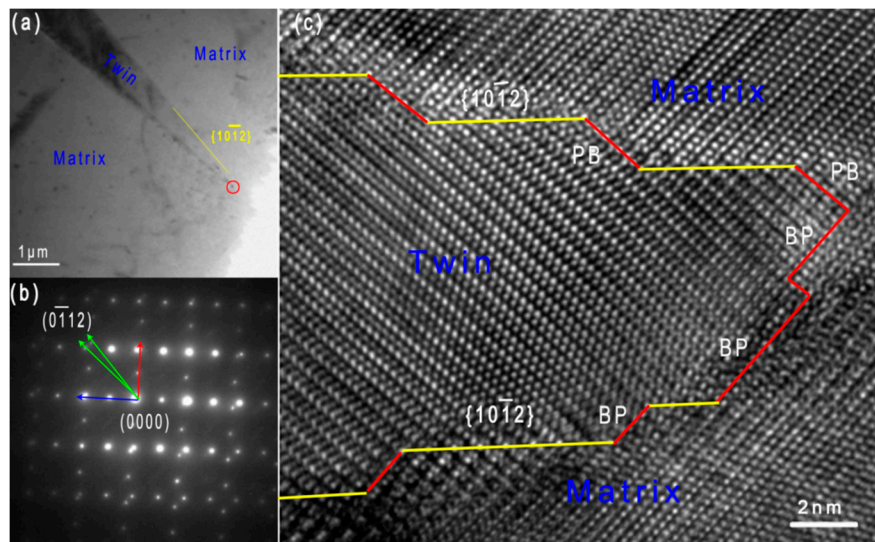
Figure 5. High resolution transmission electron microscopy image of $\{10\bar{1}2\}$ twin in magnesium containing basal-prismatic facets. (**a**) Morphology of a $\{10\bar{1}2\}$ twinning tip. The theoretical $\{10\bar{1}2\}$ twinning plane is denoted by a yellow solid line. (**b**) Selected area electron diffraction pattern of a twinning boundary along the $\langle1\bar{2}10\rangle$ zone axis. (**c**) HRTEM image of the twinning tip highlighted by a red circle in (**a**). Three kinds of facets are shown, including a straight $\{10\bar{1}2\}$ interface, a basal-prismatic and a prismatic-basal, which are marked by yellow and red lines, respectively. (Reproduced from [44], with permission from Elsevier, 2014).

It was demonstrated that facets can be nucleated by pile-up of disconnections [10–12]. Such pile-up can produce a disclination, which is settled in the facet junctions and accommodates the misorientation difference between facets. This mechanism was demonstrated by Ostapovets and Gröger by using atomistic simulations for the case of $\{10\bar{1}2\}$ twin in Mg [12]. More general theoretical analysis was provided by Barrett and El Kadiri [10,11], who predicted possible faceting on $\{10\bar{1}1\}$, $\{10\bar{1}2\}$ and $\{10\bar{1}3\}$ twin boundaries in hcp. These authors demonstrated that dislocation pile up can lead to nucleation of basal-prismatic $(0001)/\{10\bar{1}0\}$ or conjugate twin $\{10\bar{1}2\}$ (K_2) interfaces in the case of $\{10\bar{1}2\}$ twinning; basal-pyramidal $(0001)/\{10\bar{1}1\}$, pyramidal-pyramidal $\{10\bar{1}1\}/\{10\bar{1}3\}$ or conjugate $\{10\bar{1}3\}$ twin interfaces in the case of $\{10\bar{1}1\}$ twin. The facets predicted for the $\{10\bar{1}3\}$ twin are of the same type as for the $\{10\bar{1}1\}$ twin. The only difference is interchanging of K_1 and K_2 planes. It is worth noting that such faceting was observed experimentally, e.g., Figure 6 shows an example of faceted in $\{10\bar{1}3\}$ twin boundary in cobalt [51]. The boundary contains $(0001)/\{10\bar{1}1\}$ and $\{10\bar{1}1\}$ facets. The $\{10\bar{1}1\}/\{10\bar{1}3\}$ facets were reported in $\{10\bar{1}1\}$ twins in Ti [19] and in $\{10\bar{1}1\}$ twin in AZ twin in AZ31 magnesium alloy [52]. Basal-pyramidal facets were also observed in $\{10\bar{1}1\}$ twins in magnesium [13]. The segments

of K_2 conjugate twin facets were also experimentally observed in the tips of $\{10\bar{1}2\}$ twins in Zn [50] and Mg [14].
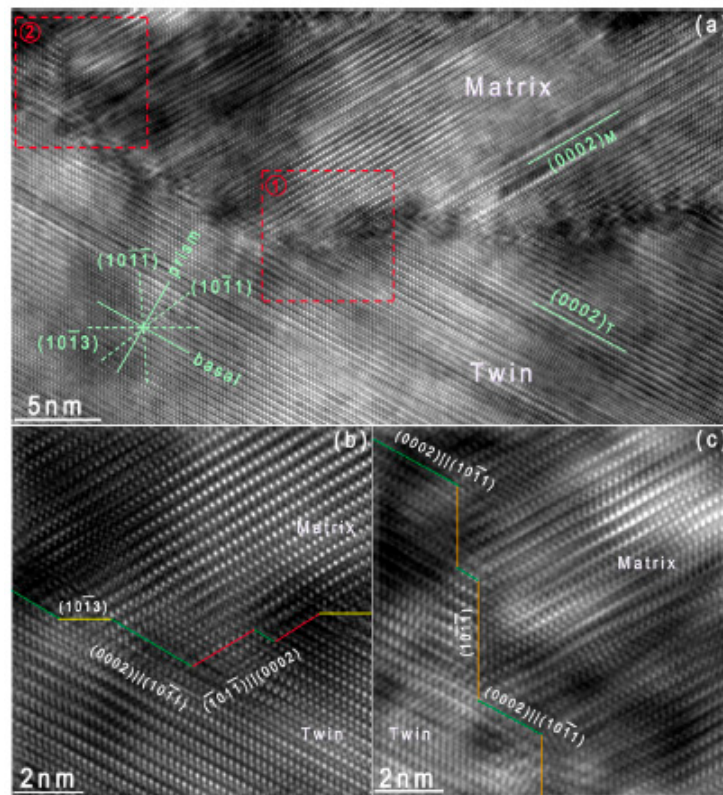

Figure 6. (**a**) High-resolution transmission electron microscopy showing the morphology of $(10\bar{1}3)$ twinning boundary. Two positions marked with the red rectangular boxes 1 and 2 in (**a**) are shown in (**b**) and (**c**), respectively, at a higher magnification. In (**b**,**c**), the 1013 twinning boundaries are denoted by the yellow lines, and the $(10\bar{1}1)$ twin facets are indicated by the orange lines. The $(0002)\|(10\bar{1}1)$ basal–pyramidal interfaces and $(0002)\|(10\bar{1}1)$ pyramidal–basal interfaces are colored in green and red, respectively. (Reproduced from [51], with permission from Elsevier, 2015).

The examination of the disconnection in Figure 2 reveals the fact that its core contains the short segment of basal-prismatic interface. Consequently, the "pile up" of several disconnections gliding in parallel planes can produce basal-prismatic facet in quite natural way as it is demonstrated in Figure 7. It is worth noting that long facet can migrate by gliding of disconnection along it. Such disconnection can incorporate into the neighboring facet when it reaches the facet junction, as it was demonstrated in [10,11,53]. Barrett and El Kadiri [10,11] have shown that such incorporation can easily lead to conversion between facets due to the topological properties of disconnections. This process is illustrated in Figures 8 and 9. Recently, conversion of basal-prismatic interface into coherent $\{10\bar{1}2\}$ twin boundary by rearrangement of disconnections was directly observed in rhenium nanocrystals by in-situ high resolution transmission electron microscopy [54]. The process was observed during growth of twin embryo, which was initially bounded by basal-prismatic interfaces.
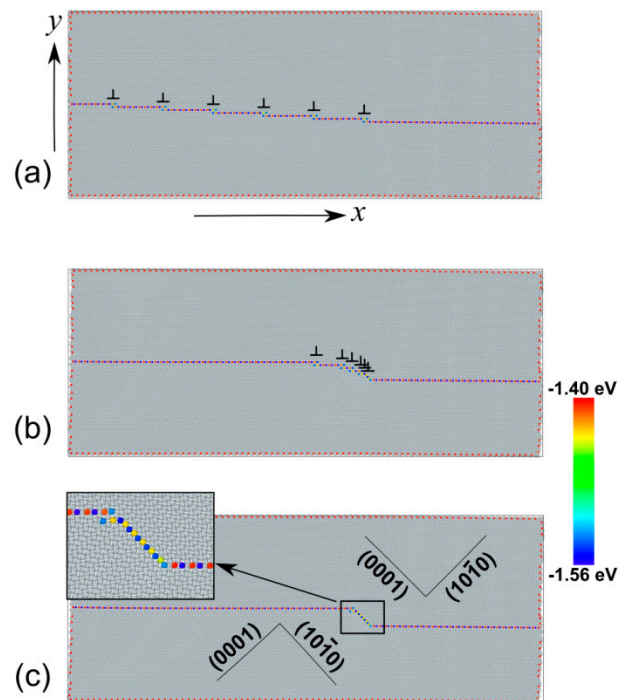
Figure 7. Formation of basal-prismatic facet in $\{10\bar{1}2\}$ twin by pile-up of disconnections in atomistic simulations: (**a**) an initial configuration of the atomic block with six disconnections (no strain applied); (**b**) the block after $\epsilon_{xy} = 1.5\%$; (**c**) the block after $\epsilon_{xy} = 3\%$ showing the formation of the basal-prismatic interface. Projection in the $[1\bar{2}10]$ direction. (Reproduced from [12], with permission from IOP publishing, 2014).
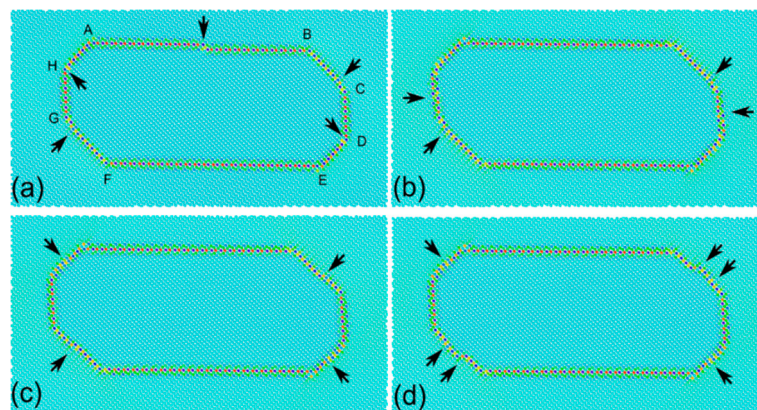

Figure 8. Different stages of twin embryo growth under applied shear strain. The faceted $\{10\bar{1}2\}$ twin embryo is bounded by K_1 twin boundaries (AB and FE), basal-prismatic facets (AH, BC, DE, FG) and conjugate $\{10\bar{1}\bar{2}\}$ K_2 boundaries (CD and HG). Arrows point to disconnections. (**a**) Initial relaxed configuration with one disconnection in the $\{10\bar{1}2\}$ boundary and one disconnection in two basal-prismatic boundaries; (**b**–**d**) Different stages of twin growth under applied shear strain. Arrows point to disconnections. (Reproduced from [53], with permission from Taylor & Francis Ltd., 2014).
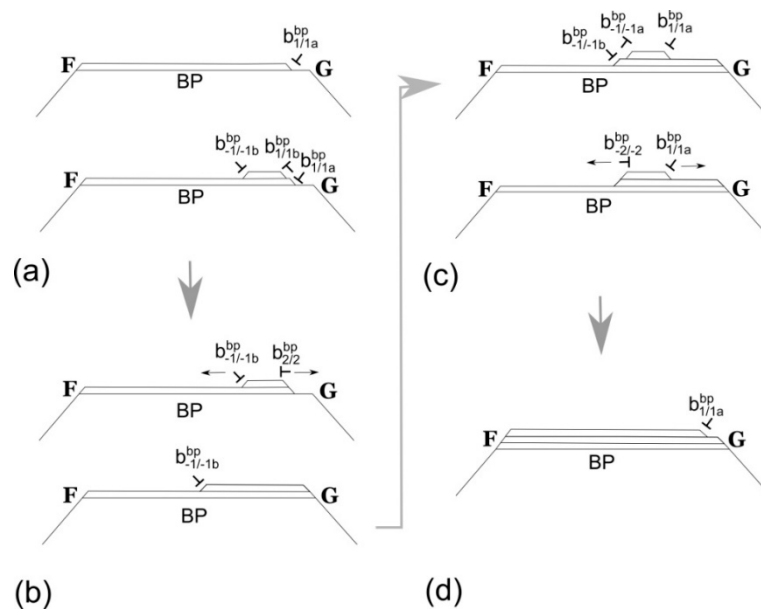
Figure 9. Scheme of FG facet migration with subsequent growth of neighbor facets due to incorporation of gliding disconnections step into them. (**a**) Nucleation of $\mathbf{b}_{1/1}^{bp}$ disconnection dipole in the BP facet nearby existing disconnection; (**b**) Interaction between two $\mathbf{b}_{1/1}^{bp}$ facets with production of $\mathbf{b}_{2/2}^{bp}$ disconnection, which is absorbed in facet junction G; (**c**) Nucleation of another $\mathbf{b}_{1/1}^{bp}$ disconnection dipole nearby existing disconnection and subsequent nucleation of $\mathbf{b}_{2/2}^{bp}$ disconnection; (**d**) Absorption of $\mathbf{b}_{2/2}^{bp}$ disconnection in facet junction F. (Reproduced from [53], with permission from Taylor & Francis Ltd., 2014).

The mechanism of facet formation due to pile up of disconnections can lead to formation of conjugate twin facets as discussed above. The interesting consequence of this mechanism takes place for the case of so-called type I and type II twins. The twin modes with rational K_1 and K_2 planes are called compound twins. However, in some cases, one of these planes can be a plane with irrational indices. The twin with rational K_1 and irrational K_2 plane is called type I twin. Correspondingly, the twin with irrational K_1 and rational K_2 plane is called type II twin. It is clear that type I and type II twins are conjugate to each other. It was recently proposed that the formation of irrational type II twin interfaces can be interpreted as a pileup of disconnections gliding on rational planes [55,56] It was proposed that type I twins form preferentially when the ratio $\dot{G}/\dot{N}$ is sufficiently large, and type II for lower values $\dot{G}$ represents the twin growth rate, which is dominated by the disconnection mobility on the K_1 glide plane, and $\dot{N}$ is the nucleation rate of disconnection pairs on this plane.

The previous analysis considered two-dimensional faceting of twins. Some recent papers also reported three -dimensional faceting [57,58]. The boundary lateral to the shear direction of the twin is hard to observe by electron microscopy due to its crystallography. Liu et al. [57] characterized lateral boundaries of $\{10\bar{1}2\}$ deformation twins in magnesium. It was found that the boundary is serrated and comprised of $\{10\bar{1}2\}$ coherent twin boundaries and semi-coherent twist prismatic–prismatic $\{2\bar{1}\bar{1}0\}$ boundaries that control twin growth. Liu et al. [58] provide statistical analysis of twin shapes viewing along three orthogonal directions: the view along the twin shear direction (η_1), the twinning plane normal view (k_1) and the view along the direction λ ($\lambda = k_1 \times \eta_1$). It was shown that twins in the η_1 and λ views normally exhibit a lenticular shape, whereas they show an irregular shape in the twinning plane normal view. It was also found that twins grow faster along λ the lateral direction than along η_1 the forward propagation direction at the initial stages of twin growth. These twin sections are irregular, indicating that growth is locally controlled and the overall shape is not perfectly ellipsoidal.

Such behavior can be explained by differences in the mobility of the edge and screw components of the twinning disconnections [58,59].

Another way of facet nucleation is the interaction of the coherent twin boundary with a crystal dislocation. Serra and Bacon [29] reported one example of such nucleation at the {$10\bar{1}2$} twin boundary when it interacts with a 60° <*a*> dislocation. The dislocation is absorbed by the interface and it is transformed into n disconnections, whose core is shown in Figure 2b, that glide away and a basal/prismatic facet with Burgers vector ***b***. The conservation of the Burgers vector during the reaction relates the total number of gliding disconnections "*n*" with the magnitude of ***b***, which is related to the length of the facet. The reaction is the one with smaller magnitude of ***b***, which depends on the *c/a* ratio (*n* = 3 for Mg, Ti and Zr). This study was in agreement with a pioneering experimental research by Lay and Nouet on the study of {$10\bar{1}2$} twin deviating from exact orientation in zinc and magnesium [36,60] and the morphology of {$10\bar{1}2$} twins in zinc and related interfacial defects [37,38].

4. The {$10\bar{1}2$} Deformation Twinning

The main peculiarity of {$10\bar{1}2$} twin, compared with the other twins in hcp metals, is that this twin is the most frequent in metals like magnesium or cobalt. However, macroscopic shape of the twin often differs from the typical straight lamella [46,61,62] due to the existence of non-invariant facets such as basal-prismatic [18,44]. This non-standard shape stimulated the development of new theories. These theories claim, for instance, zero shear produced by this mode, pure shuffle mechanisms of its growth without acting of disconnection etc. However, the growth mechanisms of this twin at the atomic level are the same as for any other twin in the hcp metals. In the following, we show that the classical theory explains in a systematic manner all phenomena covered by the new theories.

4.1. Twinning Shear of {$10\bar{1}2$} Twin Mode

A dispute on the value of shear for the {$10\bar{1}2$} twin appeared in the recent literature. This fact is surprising since the study of this frequent twinning mode has long history [2,7]. However, dozens of papers have considered this topic in the last five years. For instance, Li and Zhang [28] postulated: "Twinning shear should be zero for {$10\bar{1}2$} mode because of the breakdown of the invariant plane strain condition, which is a fundamental assumption in classical twinning theory." This claim was based on the observation of basal-prismatic facets on {$10\bar{1}2$} boundaries and on the observation of the transformation twin-parent through the migration of basal-prismatic interfaces in micro-pillar experiments [63].

The zero-shear claim invoked new experimental verification of the shear value by Molodov et al. [64] that provided a direct measurement of the twinning shear. The amount of twinning shear for {$10\bar{1}2$} twins was determined directly from the deflection of marker lines to be *s* = 0.126, in excellent agreement with the theoretical value.

The authors of [30] replied to the direct measurement of shear by the claim that "deflection will most likely be observed after twinning as a result of the one-to-one lattice transformation, but such deflection does not indicate a finite twinning shear which should be unique-valued and must occur on the first invariant plane" [65]. The last statement is based on the idea that "the actual twin boundary can be extremely incoherent on the atomic scale" and microscopically the deformation is different from simple shear (the authors of [30,65] even claim zero value of shear).

In principle, macroscopic shear can occur in this case as some kind of averaging of local values. However, zero microscopic shear value unlikely results into finite and well-defined macroscopic shear. Consequently, this value (*s* = 0.126) should occur as consequence of microscopic twinning mechanism.

It was proposed [30,63,66,67] that twinning proceeds either through "pure shuffling" or (another term for the same process) by basal-prismatic "unit cell reconstruction". These propositions were inspired by observations of basal-prismatic interface in {$10\bar{1}2$} twins. The mechanism is illustrated in Figure 10 [63]. It converts basal plane of parent crystal into prismatic plane of twin and vice versa. It is

worth noting that tetragonal transformation was recently reported as first stage of twin nucleation in rhenium [54].
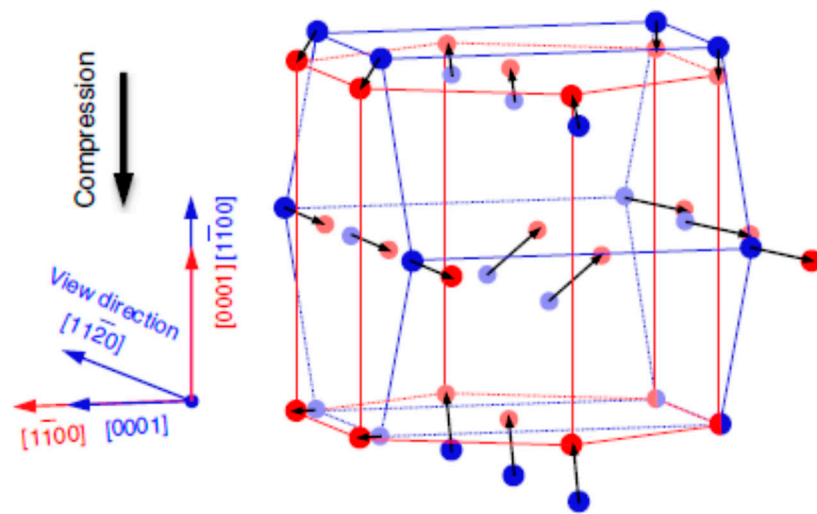

Figure 10. Transformation from parent hcp (blue) to twin hcp (red) via shuffling atomic rearrangement (Reproduced from [63], with permission of Springer Nature, 2014).

The tetragonal transformation shown in Figure 10 corresponds to the following deformation gradient [68]:

$$F = \begin{pmatrix} 1 & 0 & 0 \\ 0 & \frac{c/a}{\sqrt{3}} & 0 \\ 0 & 0 & \frac{\sqrt{3}}{c/a} \end{pmatrix} \tag{1}$$

The matrix *F* is obviously the plane unimodular deformation and consequently can be decomposed to a combination of simple shear and rotation as it was proven in [69]:

$$F = QG = Q(I + s\boldsymbol{b} \otimes \boldsymbol{m}) \tag{2}$$

It was shown [48,68,70] that simple shear *G* is exactly the shear on $\{10\bar{1}2\}$ plane with value $s = \frac{(3-(c/a)^2)}{\sqrt{3}(c/a)}$. The rotation *Q* is 3.7° about *<a>* direction of hcp lattice. This is the exact rotation necessary to put into coincidence the basal plane of the parent crystal with the prismatic plane of the twin. This process is schematically illustrated in Figure 11 [71].

Both processes, twinning shear on $\{10\bar{1}2\}$ plane and "unit cell reconstruction" shown in Figure 10 lead to the same deformation of material and to the same shear value. The difference is only in the product orientation. Such difference can be accommodated by the presence either of disclinations or the corresponding dislocation walls [53]. Figure 12 is the map of misorientation angle distribution around twin embryo. The embryo is bounded by the combination of $\{10\bar{1}2\}$ and basal-prismatic facets. The variation of misorientation shows the presence of disclinations settled in the facet junctions. It was shown in the previous section that basal-prismatic facet and core of twinning disconnection in $\{10\bar{1}2\}$ boundary are crystallographically the same.
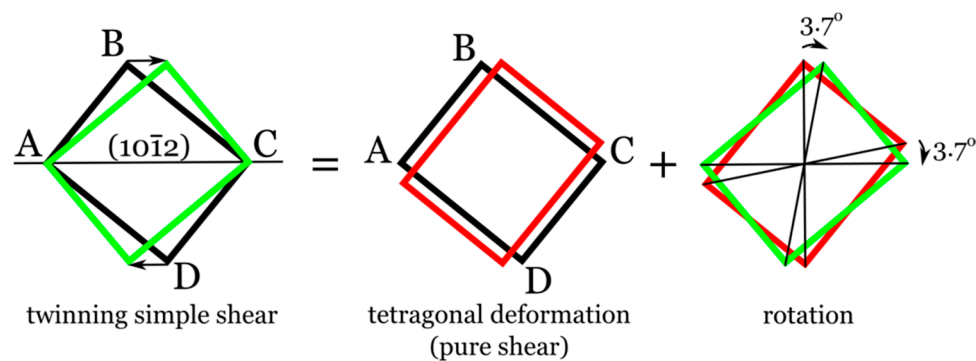
Figure 11. Scheme of interrelation between twinning simple shear on {10$\bar{1}$2} plane and basal-prismatic tetragonal deformation (from [71]). Black rectangle ABCD is the projection of hcp unit cell in <*a*> direction (AB is the trace of basal plane and BC is the trace of prismatic plane). Due to twinning shear on {10$\bar{1}$2} plane, the black rectangle is deformed into green one. Basal-prismatic tetragonal deformation deforms black rectangle to the red one. Red and green rectangles have the same shape, but different orientation (Reproduced from [71] under terms of Creative Commons Attribution 3.0 licence).
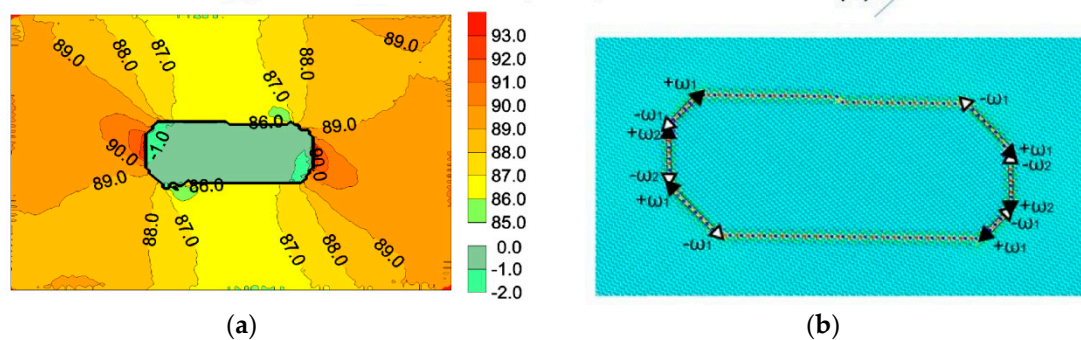
Figure 12. Variation of misorientation around faceted twin core. Distribution of lattice misorientation angle relative to the center of core (**a**) and scheme of disclinations located in the facet junctions (**b**). (Reproduced from [53], with permission from Taylor & Francis Ltd., 2014).

The exact orientation of twin relative to the parent crystal is dependent on the facet sequence as it was demonstrated in [48]. This is caused by the presence of disclinations in the facet junctions. However, the lattice correspondence and shape strain are the same in all cases. This shape strain is equivalent to the theoretical twinning shear. This shear has finite and measurable value and it is an important physical characteristic of the mechanical behavior of the material. It is worth noting that the shear value itself is independent on the shape of twin and on the twin boundary position. In this sense it is defined by the transformation shown in Figure 10, which is well known for {10$\bar{1}$2} twin mode. Such basal-prismatic transformation was proposed for this mode long time ago by Le Lann and Dubertret [72] and there was no doubt that it is compatible with the measured shear value. The breakdown of the invariant plane condition for the twin boundary plane does not mean zero shear. The change of materials shape drives the twin transformation. In this context, the boundary position is defined by the transformation mechanism but not vice versa. The classical theory used the "invariant plane condition" to predict the position of the twin boundary. However, it is obvious that the invariant plane condition gives only the simplest possible solution for the interface between parent and twin crystal. This condition cannot be satisfied for all interfaces of 3-dimensional twin and other type of interfaces can occur as it was discussed in the previous chapters. It is worth noting that the disconnection mechanism of twin growth is compatible with the breakdown of the "invariant plane condition". The dislocation nature of disconnections provides efficient way how to satisfy strain

compatibility on the "non-invariant" planes. Thus, denying the mechanism shown in [10,11,53], as the proof of the zero shear of the $\{10\bar{1}2\}$ twin [28], is an unsubstantiated speculation.

4.2. Non-Schmid Behavior

The plastic deformation is normally governed by the Schmid law. The Schmid law can be formulated in the following way [73,74]: dislocation slip would occur when the shear stress resolved on the glide plane and in the glide direction reached a critical value, the so called critical resolved shear stress (CRSS). This law is also applicable to twinning. The CRSS have to be reached on K_1 plane in η_1 direction in this case.

However, a breakdown of Schmid law was reported for some materials. The most known example of non-Schmid behavior is slip in bcc metals, where CRSS is dependent on the stress components perpendicular to the Burgers vector for glide of 1/2[111] dislocation. This phenomenon was demonstrated both theoretically [75–77] and experimentally [78,79]. Non-Schmid behavior of dislocations in bcc metals is caused by non-planar spreading of dislocation core. Due to such spreading, the core contains Burgers vector components, which are perpendicular to the total Burgers vector of dislocation. The sum of these component is zero and therefore total Burgers vector is not affected by core spreading. However, the presence of the perpendicular components leads to situation that non-Schmid stress components have influence on dislocation behavior. The deviations from Schmid law are also observed in intermetallic compounds (e.g., Ni_3Al) [80,81] with $L1_2$ structure and in atomistic simulations of screw dislocations in magnesium [82].

The non-Schmid behavior of twinning in hcp metals was also discussed in literature. However, this phenomenon is up to certain extent elusive and some authors maintained that the $\{10\bar{1}2\}$ twinning obeys the Schmid law [27]. The most notable manifestation of non-Schmid behavior was the observation of significant portion of $\{10\bar{1}2\}$ $\langle\bar{1}011\rangle$ twins with low Schmid factor [83–85]. It was proposed that such unpredictable behavior of twinning is a consequence of nucleation mechanisms, which depend on the nature of defects and their spatial organization in the crystal. For instance, Beyerlein et al. [25] pointed out that the accurate prediction of twin variants is possible when treating the nucleation in a probabilistic manner rather than by a deterministic approach based on the Schmid law. Wang et al. [86] studied twin nucleation by slip transfer in titanium. They conclude that twins activated by this mechanism always had the highest value of slip-transfer parameter (m') among the six available $\{10\bar{1}2\}$ $\langle\bar{1}011\rangle$ twinning systems, while the Schmid factor was a less significant indicator of twin activity. Through slip transfer, deformation twins sometimes formed despite having a very low global Schmid factor. The dependence of twin nucleation on non-Schmid stress components was also demonstrated by Barrett et al. [26] by modelling nucleation events under differently loaded magnesium single crystals. It was shown that non-Schmid behavior is reflected in the retardation of $\{10\bar{1}2\}$ $\langle\bar{1}011\rangle$ twins and the initial nucleation of $\{11\bar{2}1\}$ and $\langle10\bar{1}1\rangle$ twins instead. However, once $\{10\bar{1}2\}$ twins nucleated, other twins rapidly stop propagating.

Another hypothesis discussing the deviation from Schmid law for $\{10\bar{1}2\}$ $\langle\bar{1}011\rangle$ twinning, has been proposed by Cayron [87]. This hypothesis is based on a hard sphere model and claims that twinning transformation can pass through intermediate stages, which have different atomic volume from the ideal crystal. Consequently, it was claimed that the transformation path is not a simple shear, despite the fact that the initial and final configurations are the same as in the case of simple shear deformation. It was proposed to replace the Schmid law by a criterion based on a positivity of interaction work, $W = \Gamma_{ij} \times \varepsilon_{ij}$, with the usual Einstein summation convention, where Γ is the external stress field and deformation matrix ε (W is also the so-called Frobenius product between the two matrices). It is necessary to mention that this criterion does not consider critical resolved shear stress in its original form in contrast to classical Schmid law and replaces it by "critical interaction work". Probably further development of the idea is necessary in order to provide more detailed connection between critical interaction work and measurable materials parameters.

In order to calculate this interaction work, a deformation matrix that corresponds to the maximum volume change in the twinning path can be used. If the crystal is initially loaded along the c-axis direction of the hcp lattice, then one can also consider its rotation by an angle θ around the direction n normal to the $\{10\bar{1}2\}$ plane and a tilt by the angle ϕ around the $\{12\bar{1}0\}$ axis, while keeping the initial loading direction (see Figure 13). It was shown in [87] that the crystal had a positive interaction energy for tilt angles $\phi \in [-59°, 59°]$. In contrast, the calculation that used only a simple shear deformation matrix yielded positive interaction energy for a narrower tilt range $\phi \in [-43°, 47°]$. The enlarged range of tilt angles ϕ allowed for twinning can serve as possible explanation to the experimental fact that Mg twins can form for low or even negative Schmid factors. Unfortunately, the hard sphere model is quite crude model and real atomic trajectories can be more complicated than predictions of this theory. Káňa et al. [88] compared several possible transformation paths by the use of ab-initio calculations. They concluded that the application of Cayron's interaction work criterion to their paths yields to the range of tilt angle $\phi \in [-45.4°, 45.6°]$, $\phi \in [-44.6°, 42.4°]$ or $\phi \in [-43.5°, 45.8°]$, for different paths with relaxation of atomic position. These inclinations from Schmid law are smaller than predicted from hard-sphere considerations. It means that more careful consideration of atomic paths is needed for reliable predictions. It is possible to speculate that the original form of Cayron's criterion is more adequate to the case of homogeneous nucleation than to the case of twin growth. Its application to growth stage needs taking into account atomic relaxation near twin boundary and disconnection cores.
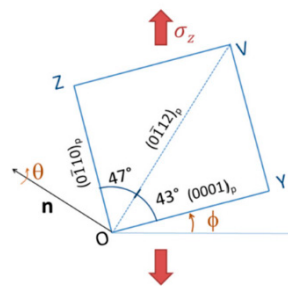

Figure 13. Scheme of loading, which is used for study of inclination from Schmid law in [87]. The definition of angles θ and ϕ is illustrated. OZVY is the projection of hcp unit cell along <*a*> hcp direction (Reproduced from [87], with permission from Elsevier, 2017).

Shear is a constant-volume deformation; so, volume changes along the transformation path can indicate that the transformation is not a simple shear in the sense mentioned by Cayron [87]. It is also worth noting that a volume relaxation is more likely to be found in the core of a twinning disconnection than in the perfect crystal. Consequently, the non-Schmid phenomena can be also treated in the dislocation description of the deformation twinning. The migration of the dislocation core through some material region can lead to reversible change of the region volume. However, the situation is more complex in this case. First of all, twin boundary itself has excess volume, i.e., volume of material nearby the boundary is different than volume in the bulk. Since twin growth is connected to the migration of the twin boundary, the passage of twin boundary through some region of material naturally leads to evolution of its volume. The excess volume of twin boundaries was studied by density functional theory (DFT), for instance in [89] for different hcp metals. All metals studied in this paper (Cd, Zn, Mg, Zr, Ti and Be) have a positive excess volume associated with the formation of $\{10\bar{1}1\}$ and $\{10\bar{1}3\}$ twin boundaries. However, the excess volume for the formation of the $\{10\bar{1}2\}$ boundary is negative for Zr and Ti and positive for Cd, Zn and Be. For the basal-prismatic interface a positive excess volume was found for Be and a negative excess volume for Zn, Cd and Zr. The excess volume of $\{10\bar{1}2\}$ and basal-prismatic twin boundaries is slightly positive and close to zero for Mg. These values are different from those predicted by considering different transformation paths [87,88]. However, it is possible to expect that Cayron's interaction work criterion can be also applicable in some sense to the twin growth stage.

The above discussion was in terms of homogeneous deformation; it was claimed [66] that non-Schmid behavior call into question that twinning is controlled by disconnections. How can we see the problem under the point of view of disconnections? To check the excess volume and atomic movements during twin boundary migration mediated by disconnection glide we have performed the following simulation.

Figure 14 shows a selected volume, which is transformed by the migration of a $\left\{10\bar{1}2\right\}$ twin boundary through it. The simulation in Figure 14 was performed using the Liu et al. [90] interatomic potential for magnesium and LAMMPS code [91]. The simulation block contained a twin boundary in its centre stepped by a disconnection as shown in Figure 14. The disconnections, due to the migration through periodic boundary conditions, transform sequentially layer by layer the matrix crystal to the twin one. The motion of disconnections was studied under an applied xy shear strain with increments of 5×10^{-5}. Energy minimization was performed after each strain increment. The corresponding atomic trajectories are shown in Figure 15a. An enlargement of the trajectories shows that they are quite complicated and differ from circular or linear as it was proposed in [87,88,92]. The trajectories consist of sections, which correspond to sweeping of subsequent atomic layers by disconnections. The atom D_0 was considered as reference. Consequently, the atomic trajectories are movements of other atoms in the unit cell relative to D_0. The atom C_0 has only shear movement, whereas N_0, L_0 and K_0 atoms are also shuffling. It is interesting that shear and shuffling take place simultaneously as it can be seen from Figure 15. The results obtained are in agreement with previous studies by Khater et al. [32] and Pond et al. [34].
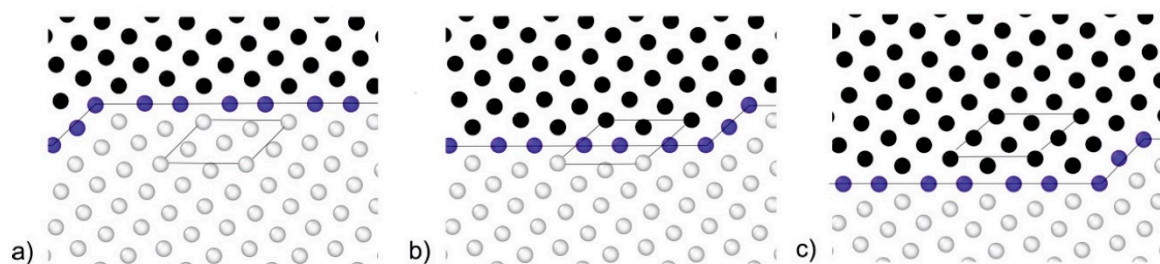

Figure 14. Passage of disconnection step through selected volume. Atoms of parent and twin crystals are shown as white and black circles, respectively. Atoms in $\left\{10\bar{1}2\right\}$ twin boundary are shown as blue circles. Parallelogram indicates selected volume. (**a**) Selected volume is located in parent crystal. Disconnection is present as step in the twin boundary. (**b**) Disconnection migrates to the right and causes twin boundary migration downwards. The twin boundary intersects selected volume. (**c**) Migration of another disconnection leads to further migration of $\left\{10\bar{1}2\right\}$ twin boundary. Selected volume is located in twin crystal now.

Thus, there is no contradiction between the description of twinning as "homogeneous deformation" and the "disconnection description". These two descriptions are two levels of approximation, but they do not contradict to each other. Possible non-Schmid behavior of disconnections needs a more detailed study. As far as we know, there are no ab-initio studies of atomic relaxations during disconnection glide in literature. The simulation shown in Figures 14 and 15 is done with quite popular empirical Liu et al. potential. It results in negative excess volume per unit surface for $\left\{10\bar{1}2\right\}$ twin boundary (-0.08 Å) and for disconnection on it (-0.04 Å). This value of excess volume per unit surface for $\left\{10\bar{1}2\right\}$ twin boundary is different from the one predicted by ab-initio calculations (about 0.02 Å) [89]. This discrepancy confirms the strong dependence of these effects on interatomic forces rather than on pure geometrical considerations.
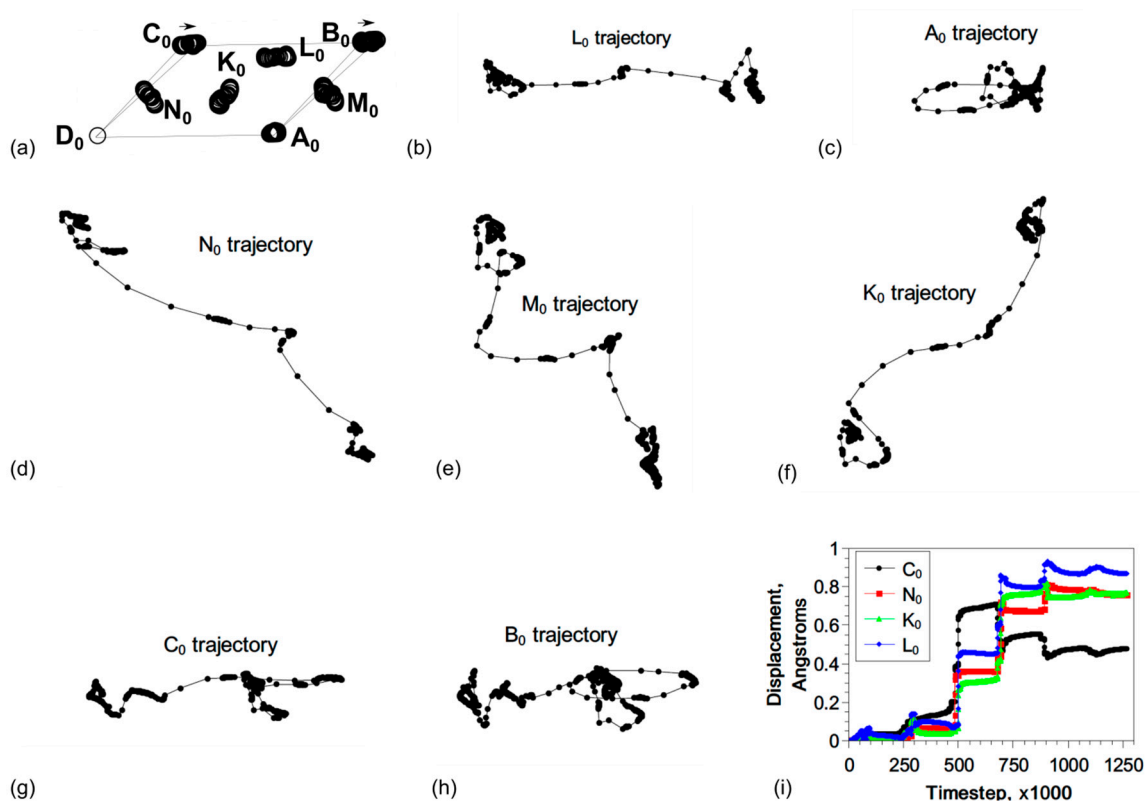
Figure 15. (**a**) General view of atomic motions during passage of disconnections through volume $A_0B_0C_0D_0$; (**b**) Trajectory of atom L_0; (**c**) Trajectory of atom A_0; (**d**) Trajectory of atom N_0; (**e**) Trajectory of atom M_0; (**f**) Trajectory of atom K_0; (**g**) Trajectory of atom C_0; (**h**) Trajectory of atom B_0; (**i**) Dependence of displacement distance on timestep for selected atoms. Shear and shuffling take place simultaneously. Trajectories are shown, relative to the atom D_0, which was taken as a reference.

5. Summary

The following experimental results published during the last decade, related to deformation twinning in hcp metals, have been presented by some authors as counterexamples of the classical theories:

1. Twin boundaries in hcp metals can be significantly inclined from the classical description that satisfy the "invariant plane conditions".

2. The observations of abundant twin boundary faceting and frequent occurrence of basal-prismatic interface in $\{10\bar{1}2\}$ twin, invoked debates on possible deviations of twinning deformation from simple shear. This idea exists in two variants: the proposition of zero shear and the proposition of non-constant volume along the transformation path, despite the fact that final twin structure is the same as in the case of twin shear.

Besides, debates on the relevance of twinning disconnections take place on the basis of the mentioned experiments.

The present review demonstrates that the findings listed above do not contradict the classical theory of twinning and they are in agreement with the disconnection mechanisms of twin growth.

"Breakdown of invariant plane condition":

The faceting of twin boundaries can be understood as "pile-up" of disconnections gliding in parallel planes. Moreover, the disconnection cores themselves often contain a short segment of one of the frequently observed facets. Consequently, the phenomenon of significant twin boundary inclination from the invariant plane fits the idea of disconnection growth mechanism. The breakdown of "invariant plane condition" on such facets is the natural consequence of the dislocation nature of disconnections.

"Claim of zero shear for $\{10\bar{1}2\}$ twin":

The breakdown of "invariant plane condition" for a given experiment does not mean zero shear (several theoretical and experimental considerations prove this statement). In fact, the product twin of this experiment is still obtained from the parent crystal by shear deformation (with value equal to the theoretical one), but the orientation of the product can be slightly different from the situation when the invariant plane condition is satisfied. In this case, a rigid rotation of the product relative to the classical position occurs. Replacement of shear twinning deformation by tetragonal Bain deformation, which was proposed in recent literature, does not lead to physically new type of deformation and it is equivalent to change of coordinate system.

"Claim of non-constant volume twinning paths":

Finally, the idea of variable volume during the transformation path is in agreement with the disconnection mechanism. The atomic paths in disconnection cores are quite complicated and each disconnection core has defined excess volume. The glide of a disconnection through some material point leads to temporary change of material volume in this point. This behavior can be important for further study of non-Schmid behavior of twins. In this context, the study of disconnection cores can be the next step towards a better approximation in comparison to the models that consider twinning as a homogeneous transformation.

Author Contributions: Conceptualization, A.O. and A.S.; writing—review and editing, A.O. and A.S.; All authors have read and agreed to the published version of the manuscript.

Conflicts of Interest: The authors declare no conflict of interest.

References

1. Cahn, R.W. Twinned crystals. *Adv. Phys.* **1954**, *3*, 363–445. [CrossRef]
2. Christian, J.W. *The Theory of Transformations in Metals and Alloys*; Pergamon Press: Oxford, UK, 1965.
3. Bilby, B.A.; Crocker, A.G. The theory of the crystallography of deformation twinning. *Proc. R. Soc. A* **1965**, *288*, 240–255.
4. Bevis, M.; Crocker, A.G. Twinning shears in lattices. *Proc. R. Soc. A* **1968**, *304*, 123–134.
5. Bevis, M.; Crocker, A.G. Twinning modes in lattices. *Proc. R. Soc. A* **1969**, *313*, 509–529.
6. Yoo, M.H.; Lee, J.K. Deformation twinning in h.c.p. metals and alloys. *Philos. Mag. A* **1991**, *63*, 987–1000. [CrossRef]
7. Christian, J.W.; Mahajan, S. Deformation twinning. *Prog. Mater. Sci.* **1995**, *3*, 1–157. [CrossRef]
8. Hardouin Duparc, O.B.M. A review of some elements for the history of mechanical twinning centred on its German origins until Otto Mügge's K1 and K2 invariant plane notations. *J. Mater. Sci.* **2017**, *52*, 4182–4196. [CrossRef]
9. Ericksen, J.L. On correlating two theories of twinning. *Arch. Ration. Mech. Anal.* **2000**, *153*, 261–289. [CrossRef]
10. Barrett, C.D.; El Kadiri, H. Impact of deformation faceting on $\{10\bar{1}2\}$ $\{10\bar{1}1\}$ and $\{10\bar{1}3\}$ embryonic twin nucleation in hcp metals. *Acta Mater.* **2014**, *70*, 137–161. [CrossRef]
11. Barrett, C.D.; El Kadiri, H. Fundamentals of mobile tilt grain boundary faceting. *Scr. Mater.* **2014**, *84*, 15–18.
12. Ostapovets, A.; Gröger, R. Twinning disconnections and basal–prismatic twin boundary in Mg. *Model. Simul. Mater. Sci. Eng.* **2014**, *22*, 025015. [CrossRef]
13. Sun, Q.; Zhang, X.Y.; Wang, Y.C.; Ren, Y.; Tan, L.; Liu, Q. Structural characterization of $\{10\bar{1}1\}$ twin boundaries in deformed cobalt. *Mater. Character.* **2016**, *116*, 44–47. [CrossRef]
14. Tu, J.; Zhang, X.Y.; Zhou, Z.M.; Huang, C. Structural characterization of $\{10\bar{1}2\}$ twin tip in deformed magnesium alloy. *Mater. Character.* **2015**, *110*, 39–43. [CrossRef]
15. Ostapovets, A.; Gornakova, A.S. On faceting of $\{10\bar{1}1\}$ and $\{10\bar{1}2\}$ twin boundaries in hcp metals. *Mater. Lett.* **2019**, *247*, 99–101. [CrossRef]
16. Braisaz, T.; Ruterana, P.; Nouet, G.; Serra, A.; Karakostas, T.; Kehagias, T. HREM Study of the $(10\bar{1}2)$ twin and defects analysis in deformed polycrystaline alpha-Titanium. *Philos. Mag. Lett.* **1996**, *74*, 331–338. [CrossRef]

17. Wang, S.; Gong, M.; Mc Cabe, R.; Capolungo, L.; Wang, J.; Tomé, C.N. Characteristic boundaries associated with three-dimensional twins in hexagonal metals. *Sci. Adv.* **2020**, *6*, eaaz2600. [CrossRef]

18. Xu, B.; Capolungo, L.; Rodney, D. On the importance of prismatic/basal interfaces in the growth of {10$\bar{1}$2} Twins in hexagonal close packed crystals. *Scr. Mater.* **2013**, *68*, 901–904. [CrossRef]

19. Li, Y.J.; Chen, Y.J.; Walmsley, J.C.; Mathins, R.H.; Dumoulin, S.; Roven, H.J. Faceted interfacial structure of {10$\bar{1}$1} twins in Ti formed during equal channel angular pressing. *Scr. Mater.* **2010**, *62*, 443–446. [CrossRef]

20. Pond, R.C. Line defects in interfaces. In *Dislocations in Solids*; Nabarro, F.N.R., Ed.; North-Holland Publishing Company: Amsterdam, The Netherlands, 1989; Volume 8, pp. 1–66.

21. Hirth, J.P. Dislocations, steps and disconnections at interfaces. *J. Phys. Chem. Solids* **1994**, *55*, 985–989. [CrossRef]

22. Capolungo, L.; Beyerlein, I.J. Nucleation and stability of twins in hcp metals. *Phys. Rev. B* **2008**, *78*, 024117. [CrossRef]

23. Wang, J.; Hirth, J.P.; Tomé, C.N. ($\bar{1}$102) Twinning nucleation mechanisms in hexagonal-close-packed crystals. *Acta Mater.* **2009**, *57*, 5521–5530. [CrossRef]

24. Wang, J.; Beyerlein, I.J.; Hirth, J.P. Nucleation of elementary {1$\bar{1}$01} and {1$\bar{1}$03} twinning dislocations at a twin boundary in hexagonal close-packed crystals. *Modelling Simul. Mater. Sci. Eng.* **2012**, *20*, 024001. [CrossRef]

25. Beyerlein, I.J.; McCabe, R.J.; Tomé, C.N. Effect of microstructure on the nucleation of deformation twins in polycrystalline high-purity magnesium: A multi-scale modeling study. *J. Mech. Phys. Solids* **2011**, *59*, 988–1003. [CrossRef]

26. Barrett, C.D.; El Kadiri, H.; Tschopp, M.A. Breakdown of the Schmid law in homogeneous and heterogeneous nucleation events of slip and twinning in magnesium. *J. Mech. Phys. Solids* **2012**, *60*, 2084–2099. [CrossRef]

27. Godet, S.; Jiang, L.; Luo, A.A.; Jonas, J.J. Use of Schmid factors to select extension twin variants in extruded magnesium alloy tubes. *Scr. Mater.* **2006**, *55*, 1055–1058. [CrossRef]

28. Li, B.; Zhang, X.Y. Twinning with zero twinning shear. *Scr. Mater.* **2016**, *125*, 73–79. [CrossRef]

29. Serra, A.; Bacon, D.J. A new model for {1$\bar{1}$02} twin growth in hcp metals. *Philos. Mag.* **1996**, *73*, 333–343. [CrossRef]

30. Li, B.; Ma, E. Atomic Shuffling Dominated Mechanism for Deformation Twinning in Magnesium. *Phys. Rev. Lett.* **2009**, *103*, 035503. [CrossRef]

31. Khater, H.A.; Serra, A.; Pond, R.C.; Hirth, J.P. The disconnection mechanism of coupled migration and shear at grain boundaries. *Acta Mater.* **2012**, *60*, 2007–2020. [CrossRef]

32. Khater, H.A.; Serra, A.; Pond, R.C. Atomic shearing and shuffling accompanying the motion of twinning disconnections in Zirconium. *Philos. Mag.* **2013**, *93*, 1279–1298. [CrossRef]

33. El Kadiri, H.; Barrett, C.D.; Tschopp, M.A. The candidacy of shuffle and shear during compound twinning in hexagonal close-packed structures. *Acta Mater.* **2013**, *61*, 7646–7659. [CrossRef]

34. Pond, R.C.; Hirth, J.P.; Serra, A.; Bacon, D.J. Atomic displacements accompanying deformation twinning: Shears and shuffles. *Mater. Res. Lett.* **2016**, *4*, 185–190. [CrossRef]

35. Capolungo, L.; Beyerlein, I.J.; Tomé, C.N. Slip-assisted twin growth in hexagonal close-packed metals. *Scr. Mater.* **2009**, *60*, 32–35. [CrossRef]

36. Lay, S.; Nouet, G. Interaction of slip dislocations with the (01$\bar{1}$2) twin interface in zinc. *Philos. Mag.* **1994**, *70*, 1027–1044. [CrossRef]

37. Lay, S.; Nouet, G. HREM study of the (01$\bar{1}$2) twin interface in zinc. *Philos. Mag.* **1994**, *70*, 261–275. [CrossRef]

38. Lay, S.; Nouet, G. Morphology of (01$\bar{1}$2) twins in zinc and related interfacial defects. *Philos. Mag.* **1995**, *72*, 603–617. [CrossRef]

39. Kvashin, N.; García-Müller, P.L.; Anento, N.; Serra, A. Atomic processes of the shear-coupled migration of {112} twins and vicinal grain boundaries in bcc-Fe. *Phys. Rev. Mater.* **2020**, *4*, 073604. [CrossRef]

40. Combe, N.; Mompiou, F.; Legros, M. Heterogeneous disconnection nucleation mechanisms during grain boundary migration. *Phys. Rev. Mater.* **2019**, *3*, 060601. [CrossRef]

41. Wang, J.; Huang, H.C. Shockley partial dislocations to twin: Another formation mechanism and generic driving force. *Appl. Phys. Lett.* **2004**, *85*, 5983. [CrossRef]

42. Narayan, J.; Zhu, V. Self-thickening, cross-slip deformation twinning model. *Appl. Phys. Lett.* **2008**, *92*, 151908. [CrossRef]

43. Marian, J.; Cai, W.; Bulatov, V.V. Dynamic transitions from smooth to rough to twinning in dislocation motion. *Nat. Mater.* **2004**, *3*, 158. [CrossRef] [PubMed]

44. Sun, Q.; Zhang, X.Y.; Ren, Y.; Tu, J.; Liu, Q. Interfacial structure of {10$\bar{1}$2} twin tip in deformed magnesium alloy. *Scr. Mater.* **2014**, *90–91*, 41–44. [CrossRef]

45. Tu, J.; Zhang, S. On the {10$\bar{1}$2} twinning growth mechanism in hexagonal close-packed metals. *Mater. Des.* **2016**, *96*, 143–149. [CrossRef]

46. Zhang, X.Y.; Li, B.; Wu, X.L.; Zhu, Y.T.; Ma, Q.; Liu, Q.; Wang, P.T.; Horstemeyer, M.F. Twin boundaries showing very large deviations from the twinning plane. *Scr. Mater.* **2012**, *67*, 862–865. [CrossRef]

47. Zhang, X.Y.; Li, B.; Tu, J.; Sun, Q.; Liu, Q. Non-classical twinning behavior in dynamically deformed Co. *Mater. Res. Lett.* **2015**, *3*, 142. [CrossRef]

48. Ostapovets, A.; Buršík, J.; Gröger, R. Deformation due to migration of faceted {10$\bar{1}$2} twin boundaries in magnesium and cobalt. *Philos. Mag.* **2015**, *95*, 4106–4117. [CrossRef]

49. Wang, J.; Liu, L.; Tomé, C.N.; Mao, S.X.; Gong, S.K. Twinning and De-twinning via Glide and Climb of Twinning Dislocations along Serrated Coherent Twin Boundaries in Hexagonal-close-packed Metals. *Mater. Res. Lett.* **2013**, *1*, 81–88. [CrossRef]

50. Braisaz, T.; Ruterana, P.; Nouet, G. Twin tip defects related to the nucleation and growth mechanisms of the twin (10$\bar{1}$2) in zinc characterized by high-resolution electron microscopy. *Philos. Mag. A* **1997**, *76*, 1. [CrossRef]

51. Sun, Q.; Zhang, X.Y.; Yin, R.S.; Ren, Y.; Tan, L. Structural characterization of {10$\bar{1}$3} twin boundaries in deformed cobalt. *Scr. Mater.* **2015**, *108*, 109–112. [CrossRef]

52. Zhang, J.; Xi, G.; Wan, X. {10$\bar{1}$1} twin boundary showing very large deviation from the theoretical one in deformed magnesium alloy. *Mater. Charact.* **2017**, *132*, 280–283. [CrossRef]

53. Ostapovets, A.; Serra, A. Characterization of the matrix–twin interface of a (10$\bar{1}$2) twin during growth. *Philos. Mag.* **2014**, *94*, 2827–2839. [CrossRef]

54. He, Y.; Li, B.; Wang, C.; Mao, S.X. Direct observation of dual-step twinning nucleationin hexagonal close-packed crystals. *Nat. Commun.* **2020**, *11*, 2483. [CrossRef] [PubMed]

55. Pond, R.C.; Hirth, J.P. Topological model of type II deformation twinning. *Acta Mater.* **2018**, *151*, 229–242. [CrossRef]

56. Pond, R.C.; Hirth, J.P.; Knowles, K.M. Topological model of type-II deformation twinning in NiTi martensite. *Philos. Mag.* **2019**, *99*, 1619–1632. [CrossRef]

57. Liu, Y.; Li, N.; Shao, S.; Gong, M.Y.; Wang, J.; McCabe, R.J.; Jiang, Y.; Tomé, C.N. Characterizing the boundary lateral to the shear direction of deformation twins in magnesium. *Nat. Commun.* **2016**, *7*, 11577. [CrossRef]

58. Liu, Y.; Tang, P.Z.; Gong, M.Y.; McCabe, R.J.; Wang, J.; Tomé, C.N. Three-dimensional character of the deformation twin in magnesium. *Nat. Commun.* **2019**, *10*, 3308. [CrossRef]

59. Zu, Q.; Tang, X.Z.; Xu, S.; Guo, Y.F. Atomistic study of nucleation and migration of the basal/prismatic interfaces in Mg single crystals. *Acta Mater.* **2017**, *130*, 310–318. [CrossRef]

60. Lay, S.; Ayed, P.; Nouet, G. A study of (01$\bar{1}$2) twin deviating from exact orientation in magnesium. *Acta Metall. Mater.* **1992**, *40*, 2351–2359. [CrossRef]

61. Molnar, P.; Jager, A.; Lejcek, P. Twin nucleation at grain boundaries in Mg–3 wt.% Al–1 wt.% Zn alloy processed by equal channel angular pressing. *Scr. Mater.* **2012**, *67*, 467–470. [CrossRef]

62. El Kadiri, H.; Kapil, J.; Oppedal, A.L.; Hector, L.G., Jr.; Agnew, S.R.; Cherkaoui, M.; Vogel, S.C. The effect of twin–twin interactions on the nucleation and propagation of {10$\bar{1}$2} twinning in magnesium. *Acta Mater.* **2013**, *61*, 3549–3563. [CrossRef]

63. Liu, B.Y.; Wang, J.; Li, B.; Lu, L.; Zhang, X.Y.; Shan, Z.W.; Li, J.; Jia, C.L.; Sun, J.; Ma, E. Twinning-like lattice reorientation without a crystallographic twinning plane. *Nat. Commun.* **2014**, *5*, 3297. [CrossRef]

64. Molodov, K.D.; Al-Samman, T.; Molodov, D.A.; Korte-Kerzel, S. On the twinning shear of {10$\bar{1}$2} twins in magnesium–Experimental determination and formal description. *Acta Mater.* **2017**, *134*, 267–273. [CrossRef]

65. Zhang, X.Y.; Li, B.; Sun, Q. On the "twinning shear" measured from line deflection. *Scr. Mater.* **2019**, *159*, 133–136. [CrossRef]

66. Li, B.; Zhang, X.Y. Global strain generated by shuffling-dominated {10$\bar{1}$2}⟨10$\bar{1}$1⟩ twinning. *Scr. Mater.* **2014**, *71*, 45–48. [CrossRef]

67. Li, B.Y.; Wan, L.; Wang, J.; Ma, E.; Shan, Z.W. Terrace-like morphology of the boundary created through basal prismatic transformation in magnesium. *Scr. Mater.* **2015**, *100*, 86–89. [CrossRef]

68. Ostapovets, A.; Molnár, P. On the relationship between the "shuffling-dominated" and "shear-dominated" mechanisms for twinning in magnesium. *Scr. Mater.* **2013**, *69*, 287–290. [CrossRef]

69. Zheng, Q.-S.; He, Q.C.; Curnier, A. Simple shear decomposition of the deformation gradient. *Acta Mech.* **2000**, *140*, 131–147. [CrossRef]

70. Namakian, R.; Voyiadjis, G.Z. An atomic displacive model for $\{10\bar{1}2\}\langle 10\bar{1}1\rangle$ twinning in hexagonal close packed metals with the emphasis on the role of partial stacking faults in formation of $\{10\bar{1}2\}$ twins. *Acta Mater.* **2018**, *150*, 381–393. [CrossRef]

71. Ostapovets, A.; Molnár, P.; Gröger, R. IOP Conference. Ser. *Mater. Sci. Eng.* **2014**, *63*, 012134.

72. Le Lann, A.; Dubertret, A. Model for $\{10\bar{1}2\}$ Twins in H.C.P. Metals. *Phys. Stat. Solids (A)* **1979**, *51*, 497–507.

73. Schmid, E. Neuere Untersuchungen an Metallkristallen. In Proceedings of the International Congress for Applied Mechanics, Delft, The Netherlands, 22–26 April 1924; pp. 342–353.

74. Schmid, E.; Boas, W. *Kristallplastizität mit besonderer Berücksichtigung der Metalle*; Springer: Berlin, Germany, 1935.

75. Duesbery, M.S.; Vitek, V. Plastic anisotropy in bcc transition metals. *Acta Mater.* **1998**, *46*, 1481–1492. [CrossRef]

76. Gröger, R.; Vitek, V. Stress dependence of the Peierls barrier of 1/2<111> screw dislocations in bcc metals. *Acta Mater.* **2013**, *61*, 6362–6371. [CrossRef]

77. Ito, K.; Vitek, V. Atomistic study of non-Schmid effects in the plastic yielding of bcc metals. *Philos. Mag.* **2001**, *81*, 1387–1407. [CrossRef]

78. Bolton, C.J.; Taylor, G. Anomalous slip in high-purity niobiumsingle crystals deformed at 77 K in tension. *Philos. Mag.* **1972**, *26*, 1359–1376. [CrossRef]

79. Gröger, R.; Chlup, Z.; Kuběna, I.; Kruml, T. Slip activity in molybdenum single crystals compressed at 77 K. *Philos. Mag.* **2018**, *98*, 2749–2768. [CrossRef]

80. Paidar, V.; Pope, D.P.; Vitek, V. A theory of the anomalous yield behaviour in L1$_2$ ordered alloys. *Acta Metall.* **1984**, *258*, 29–32.

81. Qin, Q.; Bassani, J.L. Non-Schmid yield behavior in single crystals. *J. Mech. Phys. Solids* **1992**, *40*, 813–833. [CrossRef]

82. Ostapovets, A.; Vatazhuk, O. Non-Schmid behavior of extended dislocations in computer simulations of magnesium. *Comput. Mater. Sci.* **2018**, *142*, 261–267. [CrossRef]

83. Barnett, M.R.; Keshavarz, Z.; Beer, A.G.; Ma, X. Non-Schmid behaviour during secondary twinning in a polycrystalline magnesium alloy. *Acta Mater.* **2008**, *56*, 5–15. [CrossRef]

84. Martin, E.; Capolungo, L.; Jiang, L.; Jonas, J.J. Variant selection during secondary twinning in Mg-3%Al. *Acta Mater.* **2010**, *58*, 3970–3983. [CrossRef]

85. Capolungo, L.; Marshall, P.E.; McCabe, R.J.; Beyerlein, I.J.; Tomé, C.N. Nucleation and growth of twins in Zr: A statistical study. *Acta Mater.* **2009**, *57*, 6047–6056. [CrossRef]

86. Wang, L.; Yang, Y.; Eisenlohr, P.; Bieler, T.R.; Crimp, M.A.; Mason, D.E. Twin Nucleation by Slip Transfer across Grain Boundaries in Commercial Purity Titanium. *Met. Mater. Trans. A* **2010**, *41*, 421. [CrossRef]

87. Cayron, C. Hard-sphere displacive model of extension twinning in magnesium. *Mater. Des.* **2017**, *119*, 361–375. [CrossRef]

88. Kana, T.; Ostapovets, A.; Paidar, V. The matrix–twin transition in a perfect Mg crystal: Ab initio study. *Int. J. Plast.* **2018**, *108*, 186–200. [CrossRef]

89. Kumar, A.; Wang, J.; Tomé, C.N. First-principles study of energy and atomic solubility of twinning-associated boundaries in hexagonal metals. *Acta Mater.* **2015**, *85*, 144–154. [CrossRef]

90. Liu, X.Y.; Adams, J.B.; Ercolessi, F.; Moriarty, J.A. EAM potential for magnesium from quantum mechanical forces. *Model. Simul. Mater. Sci. Eng.* **1996**, *4*, 293–303. [CrossRef]

91. Plimpton, S. Fast parallel algorithms for short-range molecular dynamics. *J. Comput. Phys.* **1995**, *117*, 1–19. [CrossRef]

92. Yu, S.; Liu, C.; Gao, Y.; Jiang, S.; Chen, Z. A rotation-shear model on the atomic motion during $\{10\bar{1}2\}$ twinning in magnesium alloys. *Mater. Lett.* **2016**, *165*, 185–188. [CrossRef]